Combustion and Flame 173 (2016) 319–324

Contents lists available at ScienceDirect

Combustion and Flame

journal homepage: www.elsevier.com/locate/combustflame

Low voltage ignition of nanoenergetic materials with a conductive paper heater for compact remote ignition system

Nam-Su Jang[a], Sung-Hun Ha[a], Ji Hoon Kim[a], Soo-Ho Jung[b], Soo Hyung Kim[a,c], Hye Moon Lee[b,*], Jong-Man Kim[a,c,*]

[a] Department of Nano Fusion Technology and BK21 Plus Nano Convergence Technology Division, Pusan National University, Busan 46214, Republic of Korea
[b] Powder & Ceramics Division, Korea Institute of Materials Science, Changwon 51508, Republic of Korea
[c] Department of Nanoenergy Engineering, Pusan National University, Busan 46214, Republic of Korea

ARTICLE INFO

Article history:
Received 12 June 2016
Revised 16 August 2016
Accepted 16 August 2016

Keywords:
Conductive paper heater
Ignition of paper
Nanoenergetic materials
Low voltage ignitor
Compact remote ignition system

ABSTRACT

A solution-processed conductive paper heater (CPH) with metallic features is used as a new class of low voltage ignitor of nanoenergetic materials (nEMs). In contrast to conventional electrothermal ignition techniques that typically require high operating voltages, the combustion of a paper substrate with a relatively low ignition point generates high thermal energy instantaneously, which makes it possible to ignite nEMs even at low voltages as low as ~1 V. In addition, the ignition and explosion properties of CPH-based low voltage ignitors are highly controllable and reproducible, mainly due to their simple fabrication and reliable electrical properties. Based on the low voltage ignition property, a compact remote ignition system is demonstrated by integrating wireless a switching circuit, portable batteries, and heater mounter in a small plastic package and operated remotely to ignite the nEMs.

1. Introduction

Over the past few decades, nanoenergetic materials (nEMs) have gained significant attention in various military and civilian applications because their stored chemical energy can rapidly be released in the form of heat and pressure upon ignition, thereby showing superior reactivity and energy density compared to their micro and bulk counterparts [1–7]. A variety of potential applications of nEMs include micropropulsion systems [8–12], pressure-driven actuators [13–17], automotive airbag propellants [18], safety and arming devices [19], and antimicrobial energetic system [20].

To supply sufficient energy that can ignite nEMs, several strategies have been considered such as flames, laser and flash pulses, and electrothermal heating [10,21–29]. Of these, electrothermal ignition based on a microheater has recently been considered as one of the most feasible ways of developing micro-ignitors [10,26–29]. This approach uses the desirable characteristics of microheaters including fast response, reliable electrothermal performance, and a small footprint.

Despite recent advances in microheater technologies, there are still some critical issues that hinder their use as micro-ignitors of nEMs in practical applications. The fabrication is quite complicated and expensive, mainly due to the multistep micromachining process involving several high-vacuum steps. In addition, a high input voltage (typically higher than a few tens of volts) is required to induce a electrical current sufficient to generate the ignition temperature of nEMs. This probably due to two reasons: (1) the temperature of a conventional microheater depends only on the Joule heating effect, which is proportional to the electrical current, and (2) considerable heat loss by conduction to the thermally conductive supporting substrate inevitably occurs, resulting in severe degradation of the voltage-to-heat conversion efficiency. This implies that the conventional micro-ignitors need to be accompanied by a bulky apparatus to supply the operation voltage, which would critically hinder the miniaturization of an nEM ignition system.

To minimize conductive heat loss, microheaters have been also fabricated in a freestanding form by entirely etching the substrate parts underneath the device [10,27]. Although this approach enables the ignition of nEMs at relatively low voltages by improving the electrothermal performance of microheaters, fabrication complexity and low production yield are unavoidable.

We present a novel approach for low voltage ignition of nEMs based on a conductive paper heater (CPH) that consists of cellulose fiber networks covered entirely with metallic features. The unique architecture of the CPH helps achieve low voltage ignition of nEMs in two ways. First, the temperature, which is elevated instantaneously after ignition of the paper substrate, can generate sufficient thermal energy to ignite the nEMs. In particular, because

* Corresponding authors: Jong-Man Kim: Department of Nanoenergy Engineering, Pusan National University, Busan 46214, Republic of Korea. Hye Moon Lee: Powder & Ceramics Division, Korea Institute of Materials Science, Changwon 51508, Republic of Korea.
E-mail addresses: hyelee@kims.re.kr (H.M. Lee), jongkim@pusan.ac.kr (J.-M. Kim).

http://dx.doi.org/10.1016/j.combustflame.2016.08.013
0010-2180/

the ignition temperature of paper is typically much lower than that of nEMs, nEMs on a CPH can be ignited at a much lower input voltage. Second, heat loss by conduction does not occur because Joule heat generated at the current paths fully contributes to triggering the ignition of the adjacent cellulose fibers, resulting in superior voltage-to-heat conversion efficiency. In addition, the advantages of a CPH also include facile and low-cost fabrication, high electrical conductivity, and simple structure. To meet the growing demand for miniaturized ignition systems, we demonstrate a compact and portable ignition system for nEMs that can be controlled remotely, based on the desirable characteristics of CPHs.

2. Experiment details

2.1. Fabrication of conductive paper heaters

Prior to the fabrication of our CPHs, aluminum (Al) paper was prepared using a simple chemical solution process reported in our previous works [30,31]. Briefly, pristine paper substrate was first fully dried by storage in a dry oven at 85 °C. The paper was immersed in a catalytic solution consisting of 5 vol% of titanium isopropoxide ($Ti(O\text{-}i\text{-}Pr)_4$) and 95 vol% of dibutyl ether ($O(C_4H_9)_2$), and subsequently dried again in inert surroundings of argon (Ar) or nitrogen (N_2). The catalytically pretreated paper was then immersed into an Al precursor ink solution of $AlH_3\{O(C_4H_9)_2\}$ for 2 h. Because all of the cellulose fibers in the paper substrate were catalytically pretreated, a very rapid decomposition of Al precursor into Al, $1.5H_2$, and $O(C_4H_9)_2$ occurred.

Highly conductive Al nanostructures, such as films and particles, were well formed on the surfaces of the cellulose fibers and densely packed into the spaces among the fibers. Consequently, highly conductive Al paper was easily and successfully prepared. CPHs were fabricated simply by cutting the prepared Al paper according to heater designs using scissors. The fabricated CPHs have the same width and thickness of ~1 mm and ~120 μm, respectively, but different lengths and geometry according to heater model.

2.2. Preparation of nanoenergetic materials

Al nanoparticles (Al NPs; NTbase Co., Ltd.) with a diameter of 81 ± 4 nm and copper oxide nanoparticles (CuO NPs; NTbase Co., Ltd.) with a diameter of 98 ± 5 nm were used as a fuel and oxidizer, respectively, because of their non-toxicity and natural abundance [11,21,28,32–34]. To synthesize Al/CuO nEMs, Al NPs and CuO NPs were first mixed together in ethanol solution with a mixing ratio of Al:CuO = 3:7 by weight. In all experiments, the mixing ratio of Al and CuO was fixed since it had been optimized in our previous works [21,28]. The mixture was then treated in an ultrasonic bath under a power of 200 W and an operating frequency of 40 kHz for 5 min to ensure complete mixing of the NPs. Finally, well-mixed Al/CuO nEMs were obtained by completely evaporating ethanol solution in a convection oven at 80 °C for 30 min.

2.3. Fabrication of remote-ignition system

Our compact remote nEM ignition system is comprised of three parts. (1) A commercially-available wireless switching circuit (Compile Technology) that allows us to remotely control a supply of the electrical current to CPH. (2) Portable batteries (9 V, Duracell) to supply the electrical power to the switching circuit and CPH. (3) A heater mounter that can hold the CPH while connecting it electrically to the portable batteries. The ignition system was fabricated by manually integrating these three parts into a single plastic package with a lid.

2.4. Characterization

Input voltage was supplied to the CPH using a direct current (DC) power supply (E3649A, Agilent Technologies) while being controlled with commercially-available software installed on a computer. The software was also used to record the electrical current flowing through the CPH in response to the applied voltage in real time. The initial electrical resistance (R_0) of the fabricated CPH was measured using a digital multimeter (U1253B, Agilent Technologies). The sheet resistance (R_s) of the prepared Al paper was measured using a four-point probe (FPP-HS 8, DASOLENG).

Detailed morphologies of the CPHs were observed using a field emission scanning electron microscope (FESEM; S4700, Hitachi).

Electrothermal properties of CPHs with and without nEMs were characterized by measuring the temperature in response to applied voltage using a thermal imaging camera (Infravision 384, Seitron) with a measurement accuracy of ±2%. The electrothermal measurements were conducted in a temperature range of 180–600 °C. Ignition and explosive processes of nEMs were monitored in real time by using a high speed digital camera (Fastcam SA3, Photron) capable of recording images at 120 K frames/s. In this case, 1 mg of Al/CuO powder mixture was gently placed on the fabricated CPH using a small spoon after precisely weighting with a microbalance. Differential scanning calorimetry (DSC) analysis was conducted in order to estimate the critical temperature needed to cause a thermal explosion of Al/CuO nEMs by examining the total heat energy.

Repetitive tape tests were performed on the fabricated CPH ($R_0 = 0.6\ \Omega$) up to 100 cycles using a 3M Scotch^{TM} adhesive tape while monitoring the change in the electrical resistance of the device using a digital multimeter.

Crystal structures of CPHs were analyzed using X-ray diffraction (XRD; Empyrean Series 2, PANalytical) with CuKα radiation.

3. Results and discussion

Figure 1a and b show SEM images of surface morphologies of paper substrate before and after the solution-based Al coating process, respectively. Compared to the pristine paper substrate, the Al paper shows microscale cellulose fibers coated conformally with Al features, clearly indicating continuous physical paths for electron transfer. Importantly, the solution-processed Al features were formed inside the paper substrate as well as on the surface, as shown in Fig. 1c, thereby resulting in superior electrical conductivity ($R_s = 50\ m\Omega/sq$). The unique morphology of the Al paper is a key contribution to generating high temperature even at low input voltages. Figure 1d depicts the proposed novel mechanism for low voltage ignition of nEMs based on CPH. In contrast to conventional microheater-based micro-ignitor technologies, Joule heat generated at the CPH contributes only to inducing the ignition of paper by raising the temperature to the ignition point of paper (typically < 250 °C). Sufficient ignition energy of nEMs is subsequently provided by high temperature generated immediately after ignition of the paper, as illustrated schematically in Fig. 1d. This means that the intermediate step ("ignition of paper") plays a key role in achieving the low voltage ignition of nEMs by providing sufficiently high thermal energy, and not depending only on Joule heat to ignite the nEMs.

Figure 2a shows changes in the electrical current and temperature of the fabricated CPH ($R_0 = 0.79\ \Omega$) in response to applied voltage. The input voltage was sequentially applied to the device with incremental steps of 0.1 V and held for 3 s. The initial time ($t = 0$ s) is defined at the moment when the temperature reaches ~180 °C. The corresponding thermal images of the device are shown in Fig. 2b. Similar to the electrothermal behavior of typical microheaters, the current was increased by increasing the input voltage, and the temperature of the device was increased

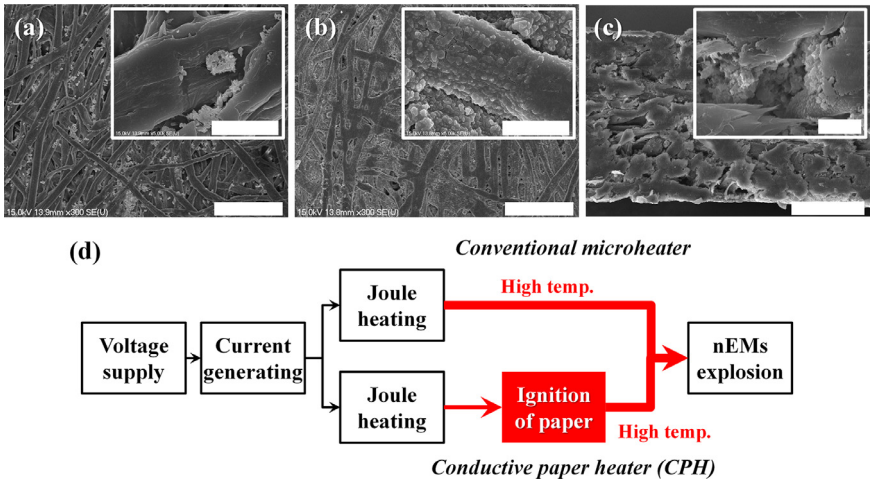

Fig. 1. Conductive paper heater. Top-view SEM images of (a) pristine paper substrate and (b) CPH, scale bars: 100 μm (inset: magnified SEM images; scale bars: 10 μm), (c) cross-sectional SEM images of CPH, scale bar: 50 μm (inset: magnified SEM images; scale bars: 10 μm), and (d) schematic flowchart showing a mechanism for low voltage ignition of nEMs using CPH.

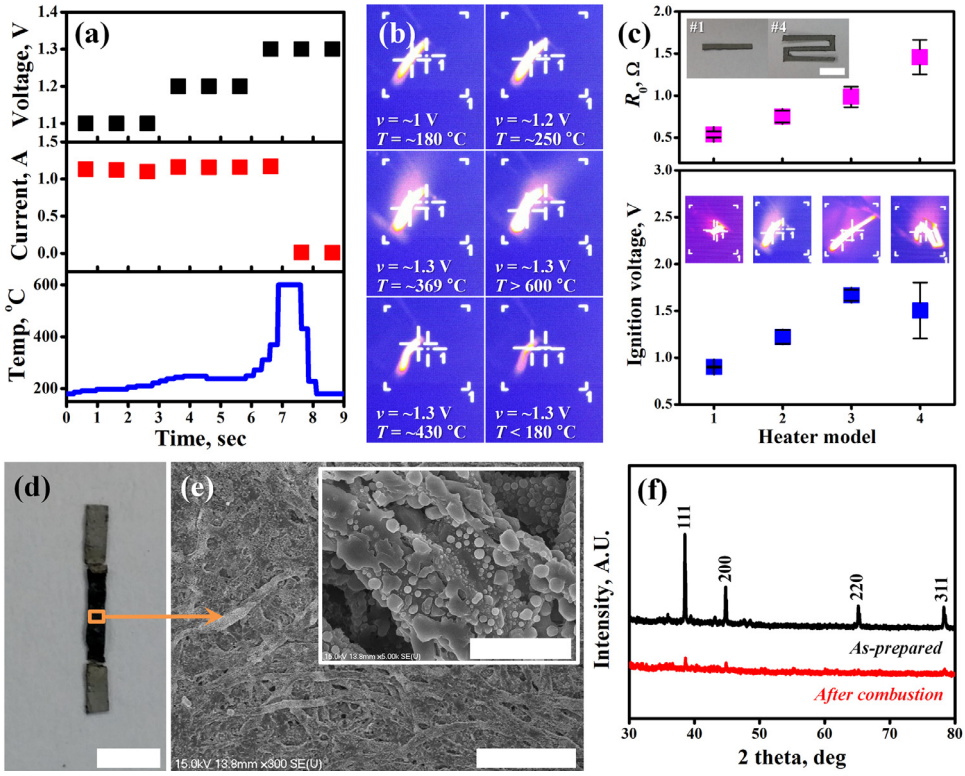

Fig. 2. Electrothermal properties of the fabricated CPH. (a) changes in the electrical current and temperature of CPH (#2) in response to applied voltage, and (b) corresponding thermal images, (c) changes in the initial resistance and ignition voltage of CPHs according to heater model (inset: digital images of the fabricated CPHs; scale bar: 5 mm, thermal images of each CPH during combustion of paper substrate), (d) digital images, scale bar: 3 mm and (e) SEM images of CPH after combustion of paper substrate, scale bar: 100 μm (inset: magnified SEM image of the burnt area; scale bar: 10 μm), and (f) XRD patterns of CPH before and after combustion of paper substrate.

accordingly by Joule heating. The temperature of the device reached ~250 °C with an applied voltage of 1.2 V, and the voltage at this point was defined as the ignition voltage of the CPH with consideration of the typical ignition point of paper. When a voltage of 1.3 V was applied, the temperature increased suddenly to greater than 600 °C. This clearly suggests that the ignition of paper by Joule heating is a direct cause of the sudden increase in temperature. Although the input voltage of 1.3 V was maintained, the temperature of the device rapidly dropped to below 180 °C within 1 s after the sudden increase occurred, showing a rapid drop in the electrical current at the same time. This is due to the fact that most of the current paths in the CPH are physically broken during the flame propagation, as shown in Fig. 2b. A CPH with a different R_0 and geometry also exhibited a similar trend in the electrothermal response except for the ignition voltage, as shown in Fig. S1 in the Supporting Information (SI).

The effect of R_0 and the geometry of the CPH on the ignition voltage was further examined using four different CPHs (models #1 ~ #4), as shown in Fig. 2c. CPHs #1 ~ #3 have a straight shape with different lengths and CPH #4 has a serpentine shape. In the case of the straight CPH model, the ignition voltage was linearly proportional to R_0. This means that a higher input voltage

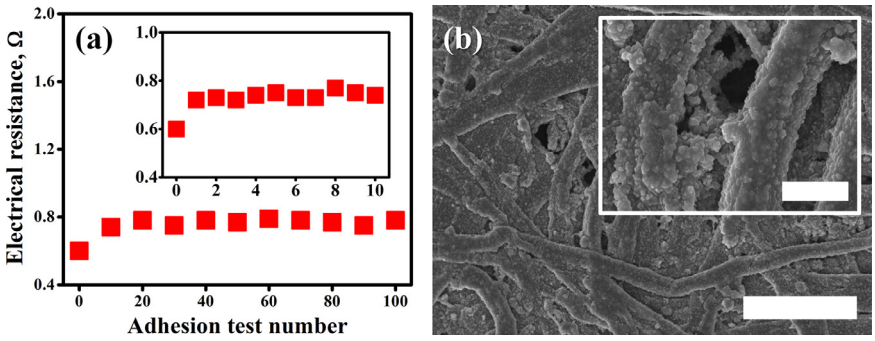

Fig. 3. Repetitive adhesion tests. (a) change in the electrical resistance of the fabricated CPH (#1) according to test number for up to 100 cycles (inset: resistance change of the device for the first 10 cycles), and (b) SEM image of the morphology of the device after repetitive adhesion tests, scale bar: 50 μm (inset: magnified SEM image; scale bar: 5 μm).

is required to induce the critical thermal ignition energy with increasing R_0 because the increase in R_0 gives rise to a decrease in current even under the same applied voltage. Interestingly, although the resistance of CPH #4 ($R_0 = 1.46 \pm 0.2\ \Omega$) is higher than CPH #3 ($R_0 = 0.99 \pm 0.12\ \Omega$), the ignition voltage tended to decrease (from 1.67 ± 0.06 V to 1.5 ± 0.3 V). This is probably due to the geometrical advantage of CPH #4 because the serpentine design is generally helpful in reducing convective heat loss to the surroundings by reducing the edge area of the device. Although there was relatively large deviation in the ignition voltages of CPHs #4 mainly due to dimensional errors occurred during cutting process, the deviation would be further reduced by using an automatic plotting system instead of manual cutting. Nevertheless, the results suggest that the electrothermal performance of the CPH can be easily optimized by controlling the geometrical designs. In particular, a very low ignition voltage of 0.9 ± 0.01 V was achieved with CPH #1 having $R_0 = 0.54 \pm 0.04\ \Omega$.

Figure 2d shows a digital image of the CPH after the combustion of paper. The burnt area became black and crumbly due to carbonization. The microstructure of the CPH at the burnt area was more precisely observed by using SEM, as shown in Fig. 2e. After being exposed at high temperature, the surface morphologies on cellulose fibers in the CPH were severely deformed compared to those of the as-prepared case (Fig. 1b). Figure 2f shows XRD patterns of the CPH before and after the combustion of paper. The XRD pattern of as-prepared CPH displays Al crystal peaks that correspond to the (111), (200), (220), and (311) planes, clearly representing the presence of Al features in the CPH. However, the intensities of the Al crystal peaks weakened significantly after the combustion of paper, as shown in the lower XRD pattern in Fig. 2f. This is probably because a considerable portion of the Al features in the as-prepared CPH was oxidized to amorphous alumina (Al_2O_3) by heat generated during the combustion of paper. This suggests that there is enough heat to provide sufficient thermal energy to ignite the nEMs.

In addition to the design flexibility, the mechanical reliability of the CPHs is one of the most important requirements in practical applications. In this regard, repetitive tape tests were conducted on the fabricated CPH (#1). Although the electrical resistance of the device was slightly increased after the first cycle, it was constantly retained while maintaining the original morphology without significant delamination of the Al features from the paper substrate, even after testing for up to 100 cycles, as shown in Fig. 3. This implies that the Al features firmly adhered to the supporting paper substrate and were conformally formed even inside the CPH, resulting in electrical robustness against repetitive physical damage.

The ignition and explosion characteristics of Al/CuO nEMs heated by the CPH were evaluated using a thermal imaging camera in order to check the usability of the CPH as a low voltage thermal ignitor of nEMs. Figure 4a shows the change in the temperature of CPH #1 loaded with Al/CuO nEMs in response to an applied input voltage. The electrothermal response is consistent with that of the CPH without nEMs. When an input voltage of 0.8 V was applied, the nEMs exploded while releasing heat and light according to the sudden increase in temperature. This means that the explosion of nEMs placed on the CPH is not dependent only on Joule heating. The entire explosion process was also visibly investigated using a high speed camera, as shown in Fig. 4b. The explosion of nEMs was found within a short period of time after ignition of paper structures in the CPH. This demonstrates that the sudden increase in temperature ($> 600\,^{\circ}C$) stemmed from the ignition of paper is an immediate cause of the explosion of the nEMs because it was experimentally confirmed that Al/CuO nEMs were thermally ignited at $\sim 532.9\,^{\circ}C$ by DSC analysis, as shown in Fig. 4c. Then, the flames spread out along the heating lines and eventually disappeared, leading to a disconnection of the current paths in the CPH. As expected, the sequential reaction was also found on a different CPH model (#4), as shown in Fig. S2 in the SI. This suggests a considerable freedom in designing heaters.

To evaluate the reproducibility of the proposed CPH-based low voltage ignition technique, 100 identical CPHs (#1) were fabricated and ignited. The voltage at the moment when the explosion occurred is defined as the explosion voltage (V_{ex}). Figure 4d shows the distributions of R_0 and V_{ex} for the 100 CPHs, which exhibit considerably uniform properties. The measured R_0 and V_{ex} were $0.66 \pm 0.07\ \Omega$ and 0.96 ± 0.08 V, respectively. Thus, the reproducible explosion performance originates from stable electrical properties of CPHs with the electrical networks formed evenly. Figure 4e shows the explosion voltage as a function of CPH model (#1–#4). The voltage shows almost the same trend as the change in the ignition voltage (Fig. 2c). This suggests that the explosion voltage of a CPH can be optimized by controlling the heater design with different R_0 values and geometry, as shown in Fig. 4e.

Figure 5a shows digital images of a miniaturized remote ignition system of nEMs, representing the three parts (switching circuit, portable batteries, and heater mounter) are integrated into a $135\ mm \times 105\ mm \times 30\ mm$ plastic package. Based on the ability to ignite nEMs at low voltages, a CPH can generate a sufficiently high temperature with portable batteries rather than bulky power supply equipment, which makes it possible to demonstrate a compact remote ignition system of nEMs. It is important to note that the proposed ignition system should be operated in ambient air so that the surrounding air can be used as an ignition source of the paper substrate.

To show the applicability of the system as a remote ignitor of nEMs in practical fields, remote explosion tests were carried out using a handheld remote controller after equipping the system

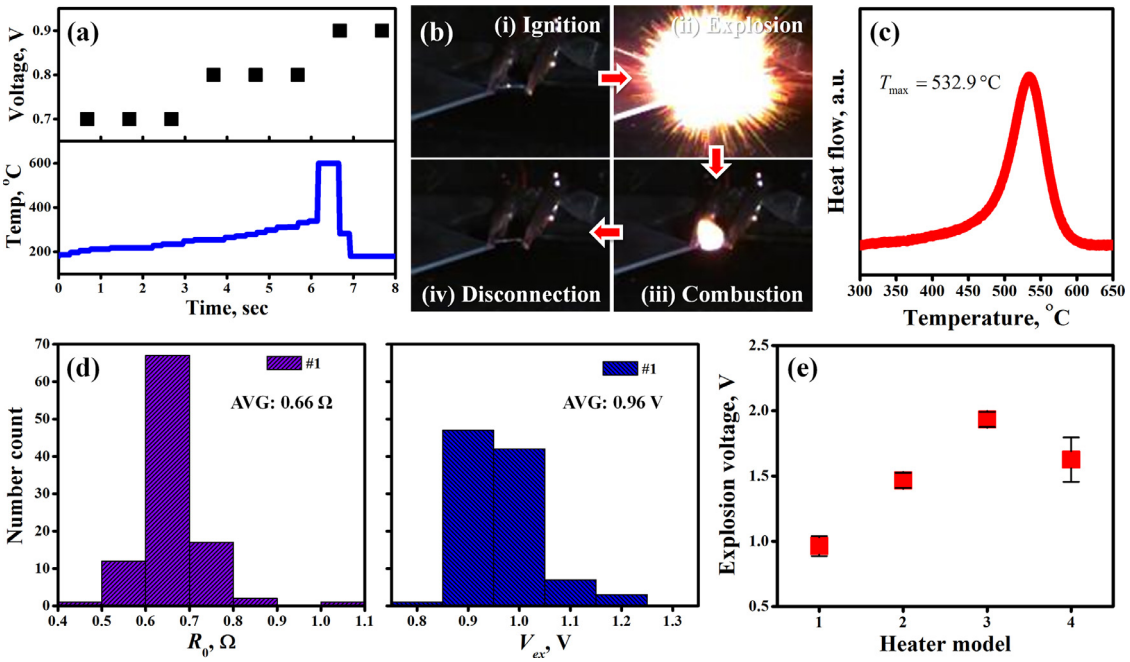

Fig. 4. Explosion properties of nEMs on CPHs. (a) change in the temperature of CPH (#1) in response to applied voltage and (b) the corresponding high-speed camera images, (c) DSC analysis results of Al/CuO powder mixture (Al:CuO = 3:7 by weight), (d) distributions of initial resistance (R_0) and explosion voltage (V_{ex}) examined on 100 identical CPHs (#1), and (e) explosion voltage of CPH as a function of heater model.

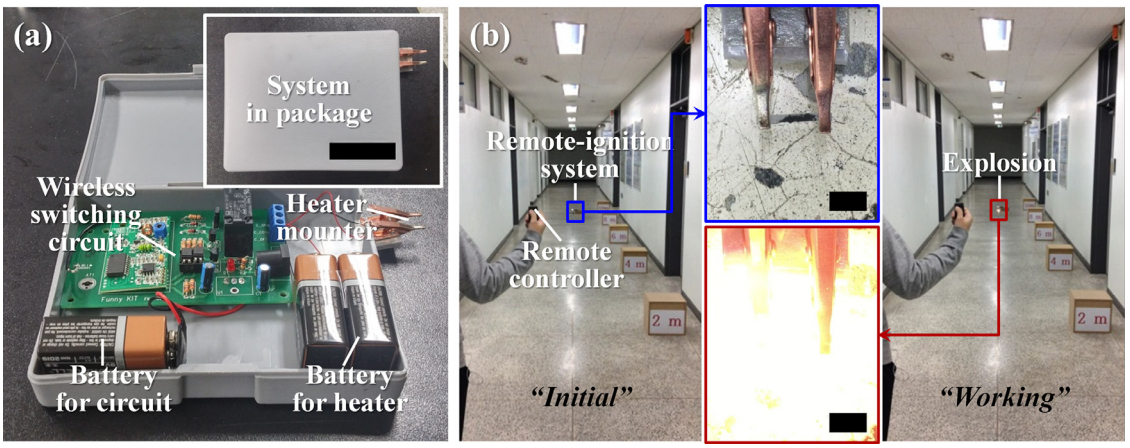

Fig. 5. Remote ignition system of nEMs. (a) digital images of remote ignition system integrated in a small plastic package (inset: digital image of the closed system; scale bar: 50 mm), and (b) digital images taken during remote explosion test that was conducted at a distance 10 m away in an open space (inset: digital images of nEMs on CPH (#1) in the initial and explosion states, scale bars: 5 mm).

with CPHs (#1) with Al/CuO nEMs. The whole explosion process was recorded in real time using a digital camera during the tests. Figure 5b shows digital images captured during a long distance (10 m) remote ignition test that was performed in an open space. When operating the remote controller, the nEMs were immediately exploded without significant time delay, as shown in Fig. 5b. In addition, a remote ignition test was conducted with an obstacle to jam the transmission of the control signals that were sent from the remote controller, as shown in Fig. S3 in the SI. The explosion of nEMs in the remote ignition system located inside a closed room was detected immediately after operating the remote controller outside. Thus, the proposed remote ignition system can be made more robust against environmental conditions that hinder the transmission of wireless signals by using high performance electronic circuits. Based on our results, we suggest that the proposed ignition system can open up new application fields because of its compactness, portability, and remote-controllability.

4. Conclusions

In this work, a novel low voltage nEM ignitor was demonstrated with a CPH. The unique architecture of the CPH with cellulose fiber networks covered conformally with Al features made it possible to ignite a paper substrate at low voltages by transferring Joule heat directly to the cellulose fibers without significant heat loss. This allowed us to generate a sufficiently high temperature to ignite the nEMs by inducing combustion of the paper substrate, resulting in low voltage ignition of the nEMs. For fixed amount of Al/CuO nEMs, the explosion voltage was controllable by changing the geometrical designs of the CPHs. 100 identical CPHs showed an initial resistance of 0.66 ± 0.07 Ω and an explosion voltage of 0.96 ± 0.08 V, representing considerable reproducibility in terms of fabrication and performance. Finally, a compact remote ignition system that can be powered by portable batteries has been demonstrated in the form of a small package, and was successfully tested

by remote control. From our experimental observations, we expect that the proposed CPH-based nEM ignition technique can be used in numerous practical applications in military and civilian fields due to superior advantages such as low voltage operation, facile and low-cost fabrication, simple architecture, reproducible performance, and remote ignitability.

Acknowledgment

This research was supported by the Civil & Military Technology Cooperation Program through the National Research Foundation of Korea (NRF) funded by the Ministry of Science, ICT & Future Planning (No. 2013M3C1A9055407).

Supplementary materials

Supplementary material associated with this article can be found, in the online version, at doi:10.1016/j.combustflame.2016.08.013.

References

[1] G. Jian, J. Feng, R.J. Jacob, G.C. Egan, M.R. Zachariah, Super-reactive nanoenergetic gas generators based on periodate salts, Angew. Chem. Int. Ed. 52 (2013) 9743–9746.
[2] F. Séverac, P. Alphonse, A. Estève, A. Bancaud, C. Rossi, High-energy Al/CuO nanocomposites obtained by DNA-directed assembly, Adv. Funct. Mater. 22 (2012) 323–329.
[3] S.H. Kim, M.R. Zachariah, Enhancing the rate of energy release from nanoenergetic materials by electrostatically enhanced assembly, Adv. Mater. 16 (2014) 1821–1825.
[4] E.L. Dreizin, Metal-based reactive nanomaterials, Prog. Energy Combust. Sci. 35 (2009) 141–167.
[5] C. Rossi, K. Zhang, D. Estève, P. Alphonse, P. Tailhades, C. Vahlas, Nanoenergetic materials for MEMS: a review, J. Microelectromech. Syst. 16 (2007) 919–931.
[6] C. Rossi, A. Estève, P. Vashishta, Nanoscale energetic materials, J. Phys. Chem. Solids 71 (2010) 57–58.
[7] X. Zhou, M. Torabi, J. Lu, R. Shen, K. Zhang, Nanostructured energetic composites: synthesis, ignition/combustion modeling, and applications, ACS Appl. Mater. Interfaces 6 (2014) 3058–3074.
[8] C. Rossi, S. Orieux, B. Larangot, T.D. Contoa, D. Estèvea, Design, fabrication and modeling of solid propellant microrocket-application to micropropulsion, Sens. Actuator A-Phys. 99 (2002) 125–133.
[9] K. Zhang, S.K. Chou, S.S. Ang, Investigation on the ignition of a MEMS solid propellant microthruster before propellant combustion, J. Micromech. Microeng. 17 (2007) 322–332.
[10] C. Rossi, D. Briand, M. Dumonteuil, T. Camps, P.Q. Phamb, N.F. Rooij, Matrix of 10×10 addressed solid propellant microthrusters: review of the technologies, Sens. Actuator A-Phys. 126 (2006) 241–252.
[11] G. Taton, D. Lagrange, V. Conedera, L. Renaud, C. Rossi, Micro-chip initiator realized by integrating Al/CuO multilayer nanothermite on polymeric membrane, J. Micromech. Microeng. 23 (2013) 105009.
[12] S. Tanaka, K. Kondo, H. Habu, A. Itoh, M. Watanabe, K. Hori, M. Esashi, Test of B/Ti multilayer reactive igniters for a micro solid rocket array thruster, Sens. Actuator A-Phys. 144 (2008) 361–366.
[13] G.A.A. Rodríguez, S. Suhard, C. Rossi, D. Estève, P. Fau, S. Sabo-Etienne, A.F. Mingotaud, M. Mauzac, B. Chaudret, A microactuator based on the decomposition of an energetic material for disposable lab-on-chip applications: fabrication and test, J. Micromech. Microeng. 19 (2009) 015006.
[14] S. Suhard, P. Fau, B. Chaudret, S. Sabo-Etienne, M. Mauzac, A.-F. Mingotaud, G. Ardila-Rodriguez, C. Rossi, M.-F. Guimon, When energetic materials, PDMS-based elastomers, and microelectronic processes work together: fabrication of a disposable microactuator, Chem. Mater. 21 (2009) 1069–1076.
[15] D.A. de Koninck, F. Molina-Lopez, D. Briand, N.F. de Rooij, Foil-level inkjet-printed pyroMEMS balloon actuators: fabrication, modeling, and validation, J. Microelectromech. Syst. 23 (2014) 1417–1427.
[16] C. Rossi, D. Estève, C. Mingués, Pyrotechnic actuator: A new generation of Si integrated actuator, Sens. Actuator A-Phys. 74 (1999) 211–215.
[17] M. Korampally, S.J. Apperson, C.S. Staley, J.A. Castorena, R. Thiruvengadathan, K. Gangopadhyay, R.R. Mohan, A. Ghosh, L. Polo-Parada, S. Gangopadhyay, Transient pressure mediated intranuclear delivery of FITC-Dextran into chicken cardiomyocytes by MEMS-based nanothermite reaction actuator, Sens. Actuator B-Chem. 171–172 (2012) 1292–1296.
[18] D. Clément, J. Diener, E. Gross, N. Künzner, V.Y. Timoshenko, D. Kovalev, Highly explosive nanosilicon-based composite materials, Phys. Status Solidi A-Appl. Mater. 202 (2005) 1357–1364.
[19] H. Pezousa, C. Rossia, M. Sanchez, F. Mathieu, X. Dollat, S. Charlot, L. Salvagnac, V. Conédéra, Integration of a MEMS based safe arm and fire device, Sens. Actuator A-Phys. 159 (2010) 157–167.
[20] K.T. Sullivan, C. Wu, N.W. Piekiel, K. Gaskell, M.R. Zachariah, Synthesis and reactivity of nano-Ag_2O as an oxidizer for energetic systems yielding antimicrobial products, Combust. Flame 160 (2013) 438–446.
[21] J.Y. Ahn, W.D. Kim, K. Cho, D. Lee, S.H. Kim, Effect of metal oxide nanostructures on the explosive property of metastable intermolecular composite particles, Powder Technol 211 (2011) 65–71.
[22] Y. Yang, Z. Sun, S. Wang, D.D. Dlott, Fast spectroscopy of laser-initiated nanoenergetic materials, J. Phys. Chem. B 107 (2003) 4485–4493.
[23] J.H. Kim, J.Y. Ahn, H.S. Park, S.H. Kim, Optical ignition of nanoenergetic materials: the role of single-walled carbon nanotubes as potential optical igniters, Combust. Flame 160 (2013) 830–834.
[24] J.H. Kim, S.B. Kim, M.G. Choi, D.H. Kim, K.T. Kim, H.M. Lee, H.W. Lee, J.M. Kim, S.H. Kim, Flash-ignitable nanoenergetic materials with tunable underwater explosion reactivity: the role of sea urchin-like carbon nanotubes, Combust. Flame 162 (2015) 1448–1454.
[25] R.W. Conner, D.D. Dlott, Time-resolved spectroscopy of initiation and ignition of flash-heated nanoparticle energetic materials, J. Phys. Chem. C 116 (2012) 14737–14747.
[26] K. Zhang, C. Rossi, M. Petrantoni, N. Mauran, A nano initiator realized by integrating Al/CuO-based nanoenergetic naterials with a Au/Pt/Cr microheater, J. Microelectromech. Syst. 17 (2008) 832–836.
[27] P. Pennarun, C. Rossi, D. Estève, D. Bourrier, Design, fabrication and characterization of a MEMS safe pyrotechnical igniter integrating arming, disarming and sterilization functions, J. Micromech. Microeng. 16 (2006) 92–100.
[28] J.Y. Ahn, S.B. Kim, J.H. Kim, N.S. Jang, D.H. Kim, H.W. Lee, J.M. Kim, S.H. Kim, A micro-chip initiator with controlled combustion reactivity realized by integrating Al/CuO nanothermite composites on a microhotplate platform, J. Micromech. Microeng. 26 (2016) 015002.
[29] S. Staley, C.J. Morris, R. Thiruvengadathan, S.J. Apperson, K. Gangopadhyay, S. Gangopadhyay, Silicon-based bridge wire micro-chip initiators for bismuth oxide–aluminum nanothermite, J. Micromech. Microeng. 21 (2011) 115015.
[30] H.M. Lee, H.B. Lee, D.S. Jung, J.-Y. Yun, S.H. Ko, S.B. Park, Solution processed aluminum paper for flexible electronics, Langmuir 28 (2012) 13127–13135.
[31] H.M. Lee, S.-Y. Choi, A. Jung, S.H. Ko, Highly conductive aluminum textile and paper for flexible and wearable electronics, Angew. Chem. Int. Ed. 52 (2013) 7718–7723.
[32] K.J. Blobaum, M.E. Reiss, J.M. Plizko, T.P. Weihs, Deposition and characteristics of a self-propagation CuO_x/Al thermite reaction in a multilayer foil geometry, J. Appl. Phys. 94 (2003) 2915.
[33] J. Shen, Z. Qiao, J. Wang, K. Zhang, R. Li, F. Nie, G. Yang, Pressure loss and compensation in the combustion process of Al–CuO nanoenergetics on a microheater chip, Combust. Flame 161 (2014) 2975–2981.
[34] P. Zhu, R. Shen, Y. Ye, S. Fu, D. Li, Characterization of Al/CuO nanoenergetic multilayer films integrated with semiconductor bridge for initiator applications, J. Appl. Phys. 113 (2013) 184505.